Uncooled low-noise thin-film optomechanical resonator for thermal sensing on lithium niobate

Yue Yu,[1,2,3,†] Ran Yin,[1,2,†] Ian Anderson,[4] Yinan Wang,[4] Jack Kramer,[4] Chun-Ho Lee,[1,2] Xinyi Ren,[1,2] Zaijun Chen,[1,2] Michelle Povinelli,[2] Dan Wasserman,[4] Ruochen Lu,[4] and Mengjie Yu[1,2,3]

[1]*Department of Electrical Engineering and Computer Sciences, University of California, Berkeley, Berkeley, CA, 94720, USA.*

[2]*Ming Hsieh Department of Electrical and Computer Engineering, University of Southern California, Los Angeles, CA, 90089, USA.*

[3]*Materials Sciences Division, Lawrence Berkeley National Laboratory, Berkeley, CA, 94720, USA*

[4]*Chandra Family Department of Electrical and Computer Engineering, The University of Texas at Austin, TX, 78712, USA*

[†]*These authors contributed equally*

1. STRUCTURAL DESIGN OF BOWL-SHAPE OPTOMECHANICAL

To reduce the optical and mechanical loss induced by the four anchors, we designed two-step etching, as mentioned in the Fabrication Section in the main text. Figure S1 shows more details of the structures after first (dark blue) and second (light blue) etching.

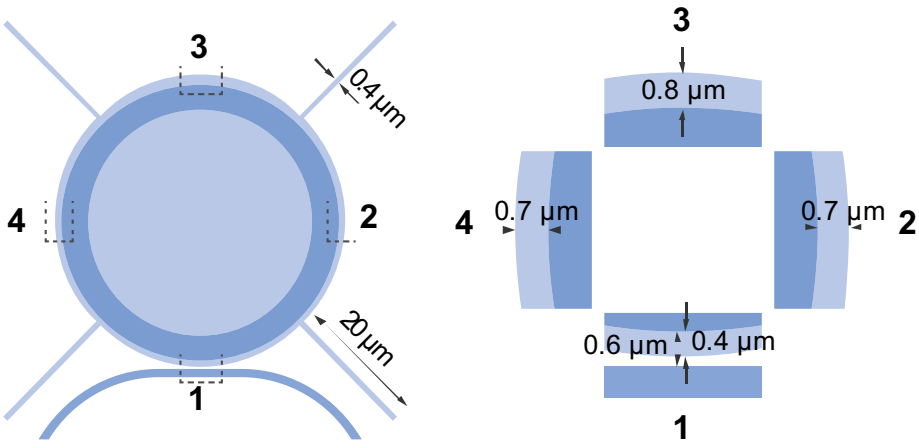

Fig. S1 | Structural design. a. Fabrication masks for the two-step etching. Blue and orange color indicate the first and second layer, respectively. **b.** Dimensions at points 1,2,3,4 as marked in **a.**

2. THERMO-OPTICAL (TO) EFFECT

Figure S2a plot the optical transmission spectrum near 1576 nm at different temperatures. As temperature increases, the resonance dip moves to longer wavelength, indicating an increase in the effective refractive index. Figure S2b plots the resonance wavelengths as a function of

temperature. A linear fit yields a TO coefficient of 3.83×10^{-5} K^{-1}. The input power was maintained at a low level to suppress potential nonlinear effects. Meanwhile, we also observed a distinct decrease in extinction ratio and increase in linewidth as temperature increases.

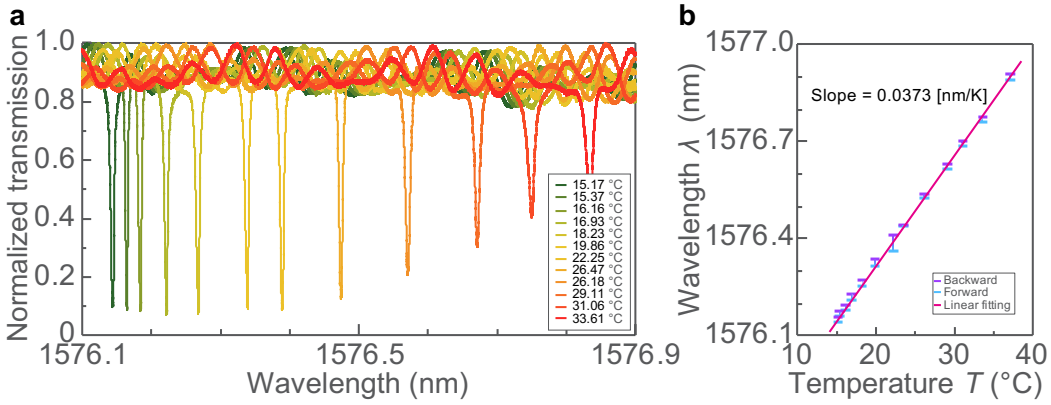

Fig. S2 | Thermo-optical measurement. a. Measured optical transmission with temperature varying from 15 to 33 °C. **b.** Resonance wavelength as a function of temperature with backward and forward sweeping.

3. SIMULATED TCFS OF DIFFERENT MECHANICAL MODES

Figure S3a plots a higher frequency mechanical signal measure through phase detection in Fig. 3c. Figure S3b plots the simulated temperature coefficients of frequency (TCFs) of four modes, where the target mode near 82 MHz shows the maximum TCFs and is consistent with experiment data.

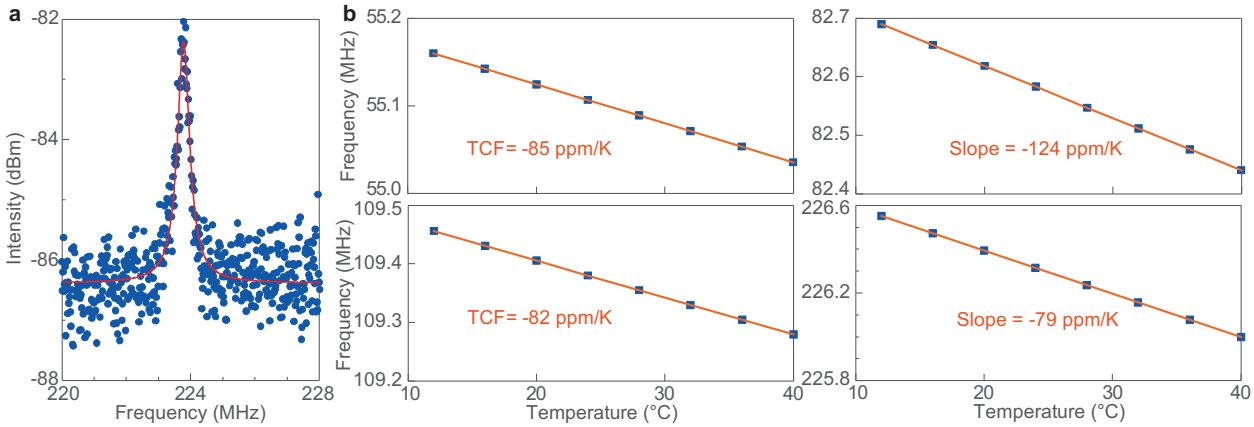

Fig. S3 | TCFs. a. Measured mechanical signal near 224 MHz. **b.** Simulated TCFs of four mechanical modes.

4. THERMAL CONDUCTANCE AND CAPACITANCE

In thermal systems, C and G_{th} are fundamental parameters that determine the dynamic and steady-state heat transfer behavior of a device. G_{th} has three main contributions: the supporting anchors, the surrounding air, and thermal radiation

$$G_{th,air} = k_{air}\frac{A_{surface}}{d}, G_{th,anchor} = 4k_{LN}\frac{A}{L}, G_{th,rad} = 4\sigma\epsilon A_{surface}T^3, (1)$$

where k_{air} and k_{LN} are the thermal conductivity of the air and LN. Asurface and A are the total surface area of the resonator and the cross section of anchors. d, L, σ, ϵ, T are the air gap between the resonator and substrate, anchor length, Stefan-Boltzmann constant, emissivity of LN, and absolute temperature. The total Gth can be written as $G_{th} = G_{th,air} + G_{th,anchor} + G_{th,rad}$. While C is defined as $\rho_{LN}c_pV$, where ρ_{LN}, c_p, and V are the LN density, specific heat capacity, and volume. Together, G_{th} and C determine the device's thermal time constant $\tau_c = C/G_{th}$. In our bowl-shaped optomechanical resonator, $A \propto wt$, $A_{surface} \propto R^2$, $V \propto Rw_rt$, where w, t, R, w_r are the anchor width, anchor (slab) thickness, the outer radius, and ring width of the resonator. By including the geometric parameters in the equations (1), we get $G_{th,air} \propto R^2/d$, $G_{th,anchor} \propto wt/L$, $G_{th,rad} \propto R^2$.

5. FREQUENCY NOISE, ALLAN DEVIATION, AND NOISE EQUIVALENT POWER (NEP)

Frequency noise, usually quantified as the power spectral density (PSD) of the frequency fluctuation $S_y(f)$, is especially important for optomechanical and sensing applications, as it determines the minimum detectable frequency shifts. Originating from different noise sources, it scales with Fourier frequency f as $S_y(f) \sim f^{\alpha}$, where α = −2, −1, ..., 2, 3 [1]. However, it doesn't directly show how stability evolves with measurement time τ. To quantify the frequency stability of a mechanical resonance over time, people use Allan deviation σ_y

$$\sigma_y^2(\tau) = 2\int_0^{\infty} S_y(f)\frac{\sin^4(\pi f\tau)}{(\pi f\tau)^2}df. (2)$$

Therefore, σ_y also follows as a power law in τ as $\sigma_y(\tau) \propto \tau^{\mu}$, where $\mu = -\frac{\alpha+1}{2}$. Note that in this paper, we consider τ within the range of 10^{-4} s to 100 s. The standard five exponents (f^2, f^1, f^0, f^{-1}, f^{-2}) are usually sufficient to describe most practical frequency noise sources in oscillators, which together result in an overall Allan deviation

$$\sigma_y(f) = \sqrt{\sum_{\alpha=-2}^{2}\sigma_{y,\alpha}^2(\tau)}. (3)$$

Among all noise sources, thermal-fluctuation-induced frequency noises establish a fundamental limit to the frequency stability of the mechanical resonator. In the following, we investigate how such thermal fluctuations contribute to frequency noise and analyze the corresponding scaling behavior σ_y with respect to τ. One is thermodynamic noise, where the temperature fluctuation $S_T(f)$ directly modulates the mechanical frequency, as

$$S_f(f) = \left(\frac{df_m}{dT}\right)^2 S_T(f), (4)$$

and $S_T(f)$ is typically Lorentzian as

$$S_T(f) = \frac{4k_B T^2 G_{th}}{(2\pi fC)^2 + G_{th}^2}, (5)$$

where kB and T are the Boltzmann constant and temperature. When $f \gg \frac{G_{th}}{2\pi C}$, $S_f(f) \propto f^0$ and $\sigma_y(\tau) \propto \tau^{-\frac{1}{2}}$, it behaves as white frequency noise; when $f \ll \frac{G_{th}}{2\pi C}$, $S_f(f) \propto f^{-2}$ and $\sigma_y(\tau) \propto \tau^{\frac{1}{2}}$, it behaves as Random-walk frequency noise. The other is thermomechanical noise, which comes from thermal forces $S_F(f)$ acting on the mechanical mode, as

$$S_f(f) = \left(\frac{g_{OM}}{2\pi}\right)^2 \frac{S_F(f)}{m_{eff}^2\left[\left(\omega_m^2 - (2\pi f)^2\right)^2 + (2\pi f \Gamma_m)^2\right]}, (5)$$

where $S_F(f) = 4k_B T m_{\text{eff}} \Gamma_m$. m_{eff}, Γ_m, and g_{OM} are the effective mass, mechanical damping rate, and optomechanical coupling rate. When $f \ll f_m$, $S_F(f) \approx$ const and $\sigma_y(\tau) \propto \tau^{\frac{1}{2}}$, which behaves as white frequency noise; when $f \gg f_m$, $S_F(f) \approx f^{-4}$ and $\sigma_y(\tau) \propto \tau^{\frac{3}{2}}$, With the above equations, we can fit the measured σ_y before and after oscillation, as shown in Fig. S4. By combining σ_y with the device G_{th} and TCF, we can convert measured frequency fluctuations into noise-equivalent power (NEP), which is a fundamental figure of merit for sensors and is defined as

$$NEP_T = \frac{\sqrt{\tau}\sigma_f(\tau) G_{th}}{TCF}. (7)$$

Optimizing the resonator geometry can help to further reduce the NEP and enhance the device performance. When operated in air, $G_{\text{th,air}}$ dominates the thermal conductance, thus the thermal fluctuation noise NEPT and thermomechanical displacement noise NEPthermo can be written as using equation (2) in the main text,

$$NEP_T \propto \sqrt{\frac{R^4}{w_r^2 t^2 d^3}}, NEP_{thermo} \propto \sqrt{\frac{R^3}{w_r t d^2}}. (8)$$

In this case, decreasing R and increasing d can substantially reduce both NEP_T and $\text{NEP}_{\text{thermo}}$ in the air. Besides, enlarging w_r and t provides additional noise suppression, though it may lead to increased optical and mechanical losses. When operated in vacuum, $G_{\text{th,air}}$ is set as 0, leaving only the anchor and radiation terms. Since $G_{\text{th,anchor}}$ and $G_{\text{th,rad}}$ are comparable, the dominant term depends on the specific structure design.

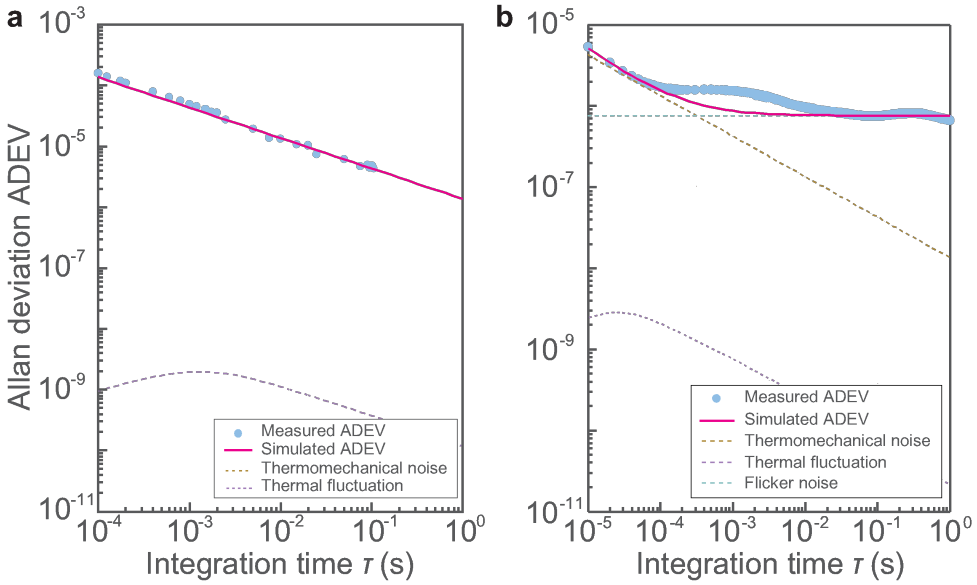

Fig. S4 | Allan deviation analysis. a. Reconstructed σ_A from oscilloscope measurement before oscillation with the fitting curves. **b.** Measured σ_A from the frequency counter after oscillation with the fitting curves.

References

[1] W. J. Riley, Nist special publication 1065: Handbook of frequency stability analysis, US Government Printing Office: Washington, DC, USA (2008).